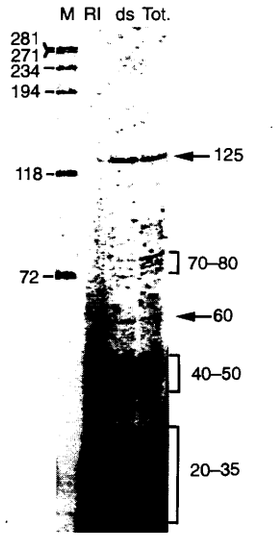

Fig. 5. Size distribution of nascent strands in yeast. (p)ppRNA-DNA chains from RI DNA and dsDNA and from total nuclear yeast DNA were radiolabeled with [α-^{32}P]GTP with the use of vaccinia guanylyltransferase (*19*). The label was removed by alkali treatment, indicating that the label was on RNA primers (*14*). The double-stranded fraction contains "full-length" Okazaki fragments of 125 nt that are not efficiently bound by BND cellulose. "Full-length" Okazaki fragments of 125 nt are absent in RI DNA, as they are already processed or ligated to leading strands. Lane M: Molecular size marker (in bases) is 0X174 RF DNA cut with Hae III.

ARS1 is flanked by the binding site of ORC, the putative initiator protein, and by element B2 (*8*) (Fig. 3B). Mutations in B2 of *ARS1* reduce replication efficiency (*3*), whereas mutations in the transition region, between B1 and B2, do not affect replication efficiency in vivo (*3*). This suggests that the transition region itself has no cis-regulatory function.

The initiation points we detected in the transition region coincide with deoxyribonuclease I–hypersensitive sites that are exposed on each strand of *ARS1* upon ORC binding in vivo and in vitro (*4*) (Fig. 3). The most pronounced hypersensitive site in element B1 (*4*) is at the transition point on the top strand. The coincidence of ORC-induced hypersensitive sites with DNA initiation sites suggests that ORC defines the transition region.

REFERENCES AND NOTES

1. B. J. Brewer and W. L. Fangman, *Cell* **51**, 463 (1987); J. A. Huberman, L. D. Spotila, K. A. Nawotka, S. M. El-Assouli, L. R. Davis, *ibid.*, p. 473; B. J. Brewer and W. L. Fangman, *Bioessays* **13**, 317 (1991); C. S. Newlon, *Microbiol. Rev.* **52**, 568 (1988).
2. V. A. Zakian, B. J. Brewer, W. L. Fangman, *Cell* **17**, 923 (1979); W. L. Fangman, R. H. Hice, E. Chlebowicz Sledziewska, *ibid.* **32**, 831 (1983); R. A. Laskey, M. P. Fairman, J. J. Blow, *Science* **246**, 609 (1989).
3. Y. Marahrens and B. Stillman, *Science* **255**, 817 (1992).
4. S. P. Bell and B. Stillman, *Nature* **357**, 128 (1992); J. F. X. Diffley and J. H. Cocker, *ibid.*, p. 169; J. F. X. Diffley, J. H. Cocker, S. J. Dowell, A. Rowley, *Cell* **78**, 303 (1994).
5. F. Jacob, S. Brenner, F. Cuzin, *Cold Spring Harbor Symp. Quant. Biol.* **28**, 329 (1964).
6. S. P. Bell, R. Kobayashi, B. Stillman, *Science* **262**, 1844 (1993); M. Foss, F. J. McNally, P. Laurenson, J. Rine, *ibid.*, p. 1838; G. Micklem, A. Rowley, J. Harwood, K. Nasmyth, J. F. X. Diffley, *Nature* **366**, 87 (1993); S. Loo *et al.*, *Mol. Biol. Cell* **6**, 741 (1995).
7. C. Liang, M. Weinreich, B. Stillman, *Cell* **81**, 667 (1995).
8. S. Lin and D. Kowalski, *Mol. Cell. Biol.* **17**, 5473 (1997).
9. J. F. X. Diffley and B. Stillman, *Proc. Natl. Acad. Sci. U.S.A.* **85**, 2120 (1988).
10. R. T. Hay and M. L. DePamphilis, *Cell* **28**, 767 (1982).
11. A. Rowley, J. H. Cocker, J. Harwood, J. F. X. Diffley, *EMBO J.* **14**, 2631 (1995).
12. RIP mapping assay on SV40 and yeast nascent DNA was performed as follows. SV40 was propagated and DNA isolated as described (*10*). SP1 yeast cells were transformed with pARS1/WTA (*3*). DNA was isolated and fractionated into dsDNA and RI DNA by BND cellulose chromatography (*7*). About 1 μg of RI DNA was heat-denatured, phosphorylated by T4 polynucleotide kinase with 50 μM adenosine triphosphate (ATP) (*10*), then incubated for 12 hours with 6 to 8 U of λ-exonuclease (Gibco) in 67 mM glycine-KOH (pH 8.8), 2.5 mM $MgCl_2$, and bovine serum albumin (50 μg/ml) at 37°C. The reaction was terminated by incubation at 75°C for 10 min. DNA was extracted once with chloroform–isoamyl alcohol. Primer extension reactions (30 μl) contained 5 ng of SV40 or 500 ng of yeast template DNA (measured by spectrophotometry before the λ-exonuclease treatment), 200 μM nucleoside triphosphates, 125 nM γ-^{32}P–labeled primer with a specific radioactivity of 10^8 cpm/μg, and 2 U of Vent (exo-) DNA polymerase (New England Biolabs) in reaction buffer [10 mM KCl, 10 mM $(NH_4)_2SO_4$, 20 mM tris-HCl (pH 8.8), 13.7 mM $MgSO_4$; modified from C. Santocanale and J. F. X Diffley, *EMBO J.* **15**, 6671 (1996)]. Thirty cycles of 1 min at 95°C, 1 min at 70°C, and 1.5 min at 72°C were performed in a Perkin-Elmer Thermocycler (Gene Amp PCR System 2400). Samples were extracted with chloroform, precipitated with ethanol, and resuspended in 3 μl of 95% formamide loading buffer. Samples were fractionated on 6% polyacrylamide–8 M urea sequencing gels. Primers used for RIP mapping were as follows: SV40/5016, 5′-CTTCATCTCCTCCTTTATCAGGATG-3′ (nt 5016 to 5040); SV40/154, 5′-CAGCAGGCAGAAGTATGCAAAGC-3′ (nt 154 to 131); rev IV, 5′-GCTTCCGGCTCGTATGTTGTGTGG-3′ (nt 617 to 640); and −90, 5′- CTGGCGAAAGGGGGATGTGCTG-3′ (nt 1032 to 1011). Nucleotide positions correspond to those in the maps shown in Fig. 3.
13. C. M. Radding, *J. Mol. Biol.* **18**, 235 (1966).
14. A.-K. Bielinsky and S. A. Gerbi, data not shown.
15. E. A. Hendrickson, C. E. Fritze, W. R. Folk, M. L. DePamphilis, *EMBO J.* **6**, 2011 (1987).
16. We constructed the plasmid pARS/A$^-$&WT by cloning a wild-type *ARS1* copy into the Aat II restriction site of the shuttle vector pARS1/858-865 (*3*). The 193-bp wild-type copy of *ARS1* (nt 734 to 926 shown in Fig. 3B) was amplified by annealing the oligonucleotides 5′-ATATATGACGTCACTCTAACAAAATAGCAAATTTC-3′ and 5′-ATATATGACGTCACAATCAATCAAAAAGCCAAA-3′, carrying an Aat II restriction site, to pARS/WTA plasmid DNA and extending them with Taq polymerase. Both ARS1 copies (active and inactive) have the same orientation.
17. S. Anderson, G. Kaufman, M. L. DePamphilis, *Biochemistry* **16**, 4990 (1977).
18. W. C. Burhans, L. T. Vassilev, M. S. Caddle, N. H. Heintz, M. L. DePamphilis, *Cell* **62**, 955 (1990).
19. M. Yamaguchi, E. A. Hendrickson, M. L. DePamphilis, *Mol. Cell. Biol.* **5**, 1170 (1985).
20. T. Nethanel, S. Reisfeld, G. Dinter Gottlieb, G. Kaufmann, *J. Virol.* **62**, 2867 (1988).
21. A. B. Blumenthal and E. J. Clark, *Cell* **12**, 183 (1977).
22. M. L. DePamphilis, *Annu. Rev. Biochem.* **62**, 29 (1993).

23. We thank C. Liang and B. Stillman for advice and yeast ARS clones, E. A. Hendrickson for the CV-1 cell line and SV40, M. L. DePamphilis for discussion, A. Landy for critical reading of the manuscript, and E. A. Hendrickson, Z. Han, and members of our laboratory for fruitful discussions. Supported by NIH grant GM 35929.

17 September 1997; accepted 13 November 1997

Modification of the NADH of the Isoniazid Target (InhA) from *Mycobacterium tuberculosis*

Denise A. Rozwarski, Gregory A. Grant, Derek H. R. Barton, William R. Jacobs Jr., James C. Sacchettini*

The preferred antitubercular drug isoniazid specifically targets a long-chain enoyl-acyl carrier protein reductase (InhA), an enzyme essential for mycolic acid biosynthesis in *Mycobacterium tuberculosis*. Despite the widespread use of this drug for more than 40 years, its precise mode of action has remained obscure. Data from x-ray crystallography and mass spectrometry reveal that the mechanism of isoniazid action against InhA is covalent attachment of the activated form of the drug to the nicotinamide ring of nicotinamide adenine dinucleotide bound within the active site of InhA.

Mycobacterium tuberculosis is particularly susceptible to isoniazid [isonicotinic acid hydrazide (INH)], the most widely used of all antitubercular drugs (*1*). Although isoniazid-based treatment regimens have been available since the 1950s, *M. tuberculosis* remains the leading cause of death worldwide from an infectious agent (*2*). Tuberculosis is now a disease associated with poverty and with acquired immunodeficiency syndrome (AIDS); the greatest impact is experienced in underdeveloped nations and in centers of urban decay (*3*). In addition, the incidence of incurable cases due to multidrug-resistant mutants is on the rise. These trends have generated renewed interest in elucidating the molecular mechanisms of action of well-established antitubercular drugs as an aid in

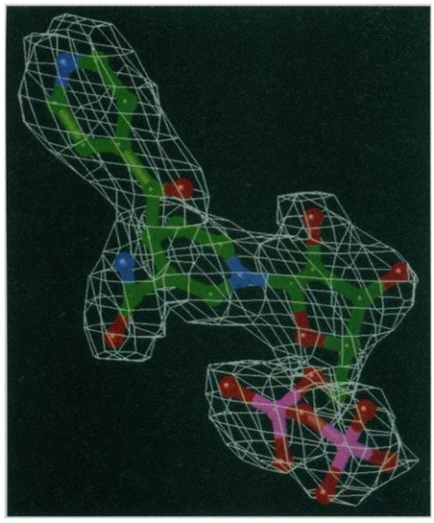

Fig. 1. A portion of the crystallographic model of the isonicotinic acyl-NADH superimposed onto the final $2F_o - F_c$ electron density map contoured at 1σ. Carbon atoms are green, oxygen atoms are red, nitrogen atoms are blue, and phosphorous atoms are magenta. Starting from the lower right, the two phosphates of NADH are in view. Moving toward the upper left is the nicotinamide ribose and nicotinamide ring of NADH. In the top left is the fragment derived from isoniazid, which retains a pyridine ring and a carbonyl group, referred to here as an isonicotinic acyl group. The isonicotinic acyl group is attached through its carbonyl carbon to the carbon at position four of the nicotinamide ring of NADH. The carbon at position four of the nicotinamide ring of the isonicotinic acyl-NADH inhibitor is tetrahedral and retains one hydrogen. Produced with the program O (*32*).

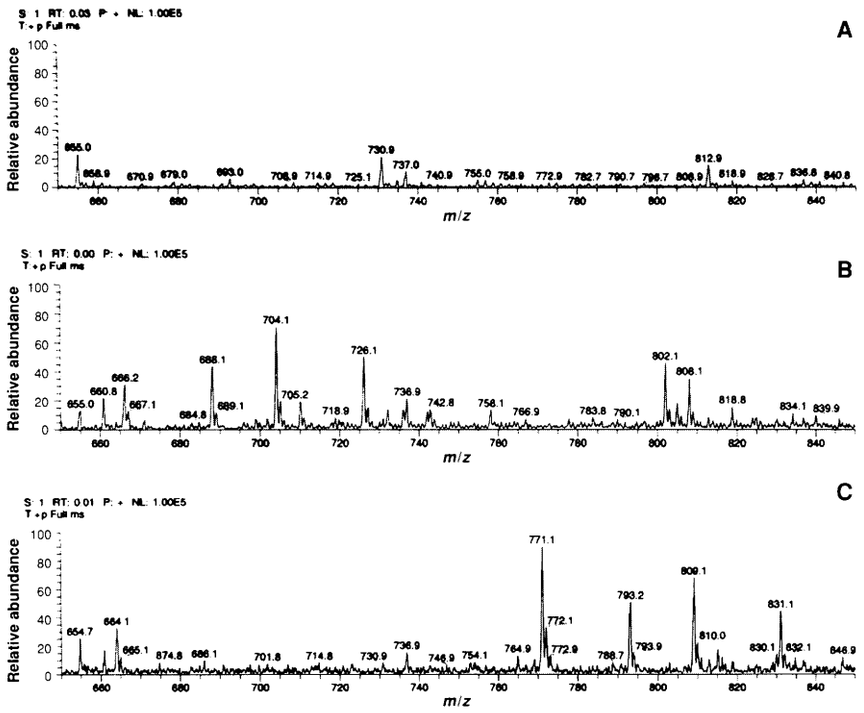

Fig. 2. Mass spectra showing that the inhibitor bound to InhA is a compound with an apparent mass of 770 daltons, which is in agreement with the chemical structure of isonicotinic acyl-NADH. (**A**) InhA alone shows no significant components within the mass/charge (*m/z*) range of 650 to 850. (**B**) InhA in the presence of NADH shows several components related to NADH. NADH displays a peak at 666 ([M + H]$^+$). Also present are adducts with one sodium ion (*m/z* = 688), with one potassium ion (*m/z* = 704), and with one sodium and one potassium ion (*m/z* = 726). Adducts with two sodium ions (*m/z* = 710) or two potassium ions (*m/z* = 742) are also present at low levels. (**C**) Isoniazid-inhibited InhA shows the absence of NADH-associated peaks and the presence of a new peak at *m/z* = 771 ([M + H]$^+$) corresponding to isonicotinic acyl-NADH. Also present are adducts with one sodium ion (*m/z* = 793), with one potassium ion (*m/z* = 809), and with one sodium ion and one potassium ion (*m/z* = 831). Adducts with two sodium ions (*m/z* = 815) or two potassium ions (*m/z* = 847) are also present at low levels. Analysis of the *m/z* peaks with Finnigan Zoomscan confirmed that they are all singly charged species.

developing new therapeutics (*4*.)

The *inhA* gene from *Mycobacterium smegmatis*, *Mycobacterium avium*, *Mycobacterium bovis*, and *M. tuberculosis* confers co-resistance to both isoniazid and ethionamide when transformed on a multicopy plasmid into *M. smegmatis* (*5*). In addition, a spontaneous laboratory-derived mutation, which results in a single amino acid substitution [Ser^{94} to Ala (S94A)] in the *M. smegmatis* and the *M. bovis* (100% identical to *M. tuberculosis*) genes, is sufficient to confer co-resistance to both isoniazid and ethionamide in *M. smegmatis* by allele exchange. Subsequent studies revealed that InhA is an enoyl-acyl carrier protein (ACP) reductase (*6*). Enoyl-ACP reductases catalyze the nicotinamide adenine dinucleotide (NADH)–dependent reduction of the double bond at position two of a growing fatty acid chain linked to ACP, an enzymatic activity common to all known fatty acid biosynthetic pathways. InhA preferentially reduces long-chain substrates (those containing 16 or more carbon atoms). Mycobacteria utilize the products of InhA catalysis to create mycolic acids, very long chain (C_{40} to C_{60}) α-branched fatty acids, which are important components of mycobacterial cell walls (*7*). In addition to the genetic data, the fact that isoniazid inhibits mycolic acid biosynthesis (*8*) and that mycolic acid biosynthesis proceeds normally in cell-free extracts of isoniazid-resistant *M. smegmatis*, due to multicopy plasmid expression of wild-type InhA or genomic expression of the S94A mutant (*5*), provides compelling evidence that InhA is the drug target for both isoniazid and ethionamide in mycobacteria.

However, isoniazid itself does not directly interact with InhA. Several lines of evidence support the theory that, to inhibit InhA, isoniazid requires conversion to an activated form of the drug and that a catalase-peroxidase (KatG) participates in isoniazid activation (*9*): (i) isoniazid, NADH (*10*), Mn^{2+} ions, and oxygen (*11*) are all required for InhA inhibition; (ii) KatG is an efficient catalyst for oxidation of Mn^{2+} ions ($Mn^{2+} \rightarrow Mn^{3+}$) (*12*) and the addition of KatG accelerates isoniazid-dependent inhibition of InhA (*13*); (iii) deletions or mutations in the KatG gene are the single largest determinant of isoniazid resistance in clinical isolates (*14*) and transformation of the KatG gene into isoniazid-resistant *M. tuberculosis* restores isoniazid sensitivity (*15*). It has been proposed that the activated form of isoniazid is an intermediate in the formation of isonicotinic acid, isonicotinamide, and pyridine-4-carboxaldehyde, the products of isoniazid oxidation, none of which inhibits InhA (*16*).

About 25% of the clinical isolates of isoniazid-resistant *M. tuberculosis* contain mutations within the promoter or structural

D. A. Rozwarski, Department of Biochemistry and Biophysics, Texas A&M University, College Station, TX 77843, USA.
G. A. Grant, Department of Molecular Biology and Pharmacology, Washington University School of Medicine, St. Louis, MO 63110, USA.
D. H. R. Barton, Department of Chemistry, Texas A&M University, College Station, TX 77843, USA.
W. R. Jacobs Jr., Department of Microbiology and Immunology and Howard Hughes Medical Institute, Albert Einstein College of Medicine, Bronx, NY 10461, USA.
J. C. Sacchettini, Department of Biochemistry and Biophysics and Department of Chemistry, Texas A&M University, College Station, TX 77843, USA.
*To whom correspondence should be addressed.

regions of the *inhA* gene, and no *inhA* mutations have been identified in isoniazid-sensitive isolates (*14*). Four different clinical isolate mutations (at residues 16, 21, 78, and 95) result in single amino acid substitutions within or near the NADH binding region of InhA (*17*). The location of the S94A mutation is also within the NADH binding region. As demonstrated by x-ray crystallography, the S94A mutant displays a reduced hydrogen bonding pattern between NADH and the enzyme (*18*), resulting in an increased Michaelis constant (K_m) for NADH (6). Isoniazid-dependent inhibition of wild-type InhA requires the presence of NADH, and inhibition of the S94A mutant occurs only when the concentration of NADH is increased (*10*), which implies that there is a correlation between the ability of the enzyme to bind NADH and to become inhibited by activated isoniazid. Furthermore, acyl-ACP substrates can prevent isoniazid-dependent inhibition of InhA, which suggests that activated isoniazid interacts with the substrate binding region of InhA (*13*).

Crystals produced from InhA inhibited by isoniazid (*19*) were isomorphous to those of the native enzyme (*18*) and were used to collect an x-ray diffraction data set to 2.7 Å resolution (*20*). The resulting difference Fourier ($F_o - F_c$) electron density map showed that the activated form of isoniazid was covalently linked to the NADH within the active site of InhA (*21*). The modified NADH consists of an isonicotinic-acyl group from isoniazid attached through its carbonyl carbon to the carbon at position four of the nicotinamide ring (Fig. 1). The isonicotinic-acyl group replaces the 4*S* (and not the 4*R*) hydrogen of NADH, which is the same position in NADH involved in the hydride transfer that occurs during reduction of enoyl-ACP substrates (6). Furthermore, the covalent attachment was verified by mass spectrometry (*22*). The mass spectrum of isoniazid-inhibited InhA reflects the presence of a compound with a molecular mass of 770 daltons, which is in agreement with the crystallographic model for the isonicotinic-acyl-NADH (Fig. 2).

Earlier proposals have suggested that isoniazid can be activated to either an isonicotinic acyl anion (*23*) or an isonicotinic acyl radical (*16*). The x-ray crystallography and mass spectrometry results show that the carbon at position four of the nicotinamide ring of the isonicotinic acyl-NADH is tetrahedral and retains one hydrogen. This suggests that formation of the isonicotinic acyl-NADH consists of addition of either an isonicotinic acyl anion to NAD^+ or an isonicotinic acyl radical to an $NAD^{\cdot}$ radical (Fig. 3). Furthermore, isonicotinic acyl-NADH formation occurs within the active site of InhA (not in

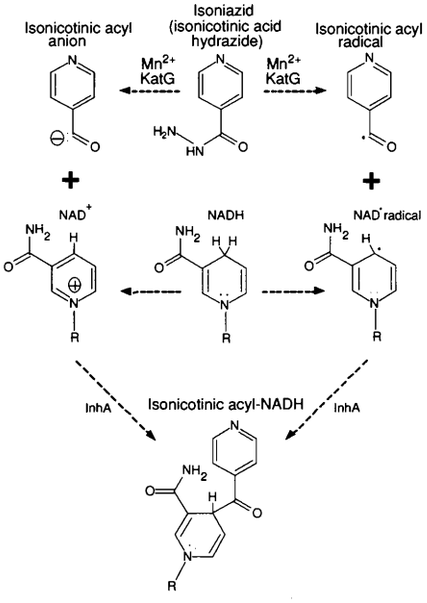

Fig. 3. Proposed pathway for formation of the isonicotinic acyl-NADH inhibitor of InhA. Two possible scenarios are shown, in which an activated form of isoniazid (isonicotinic acyl anion or radical) covalently attaches to a form of NADH (NAD^+ or $NAD^{\cdot}$ radical) within the active site of InhA, while retaining a tetrahedral carbon at position four of the nicotinamide ring. Of the two scenarios, we favor the free radical pathway because isoniazid-dependent inhibition of InhA occurs at a faster rate with NADH than with NAD^+ (*13*). Whether InhA catalyzes $NAD^{\cdot}$ radical formation is not clear, because Mn^{2+} ions are known to facilitate this process (*28*). In addition, it is likely that Mn^{3+} ions facilitate the formation of isonicotinic acyl radicals and KatG participates in isoniazid activation by increasing the rate of the conversion of Mn^{2+} to Mn^{3+} ions (*11, 12*). There are reports in the literature in which certain combinations, such as isoniazid and Mn^{2+} ions (*29*) as well as isoniazid and peroxidase enzymes (*30*), are known to generate free radical species. Furthermore, the final products of the KatG oxidation of isoniazid are likely to be formed through an isonicotinic acyl radical intermediate (*16*) and spin-trapping techniques have identified the isonicotinic acyl radical as one of the products of peroxidase-catalyzed oxidation of isoniazid (*31*). Produced with chem-D draw (*32*).

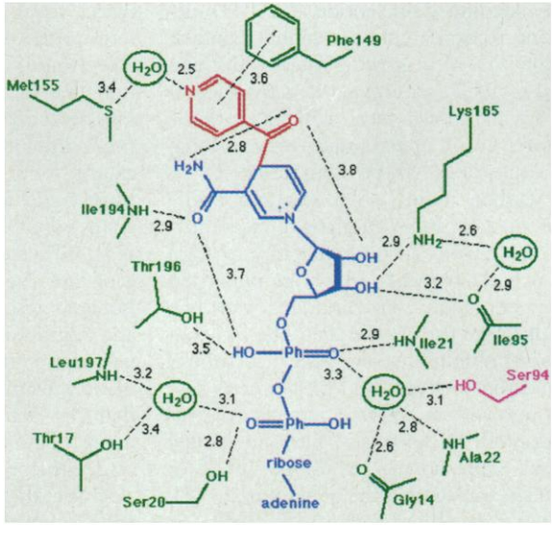

Fig. 4. Molecular contacts between isonicotinic acyl-NADH and the active site of InhA. The isonicotinic acyl group derived from isoniazid is red, the NADH portion of the analog is blue, the side chains of InhA are green, and Ser^{94}, the residue that causes isoniazid resistance when converted into Ala, is magenta. Numbers represent the distance in angstroms between selected atoms. The orientation of the isonicotinic acyl group with respect to the NADH portion of the inhibitor is such that its carbonyl oxygen is positioned about halfway between two hydrogen bond donors, the amide nitrogen of the nicotinamide ring, and the 2′-hydroxyl oxygen of the nicotinamide ribose ring. In addition, the nitrogen atom of the isonicotinic acyl group is within hydrogen-bonding distance of a buried water molecule held by the side chain of Met^{155}. The pyridine ring of the isonicotinic acyl group is surrounded by hydrophobic residues, which include Phe^{149}, Gly^{192}, Pro^{193}, Leu^{218}, Tyr^{158}, and Trp^{222}.

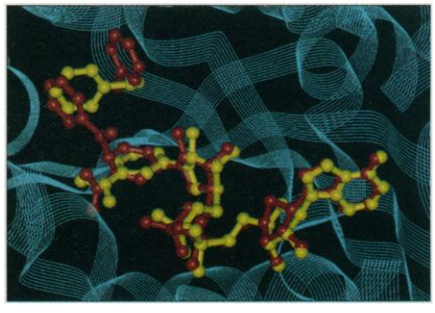

Fig. 5. Superposition of the active sites of InhA with bound NADH (yellow) and with bound isonicotinic acyl-NADH (red). The only conformational difference between the active sites is displacement of the side chain of Phe^{149}. In the native enzyme, NADH binds at the bottom of a large open cavity, and the side chain of Phe^{149} lies immediately above the nicotinamide ring, appearing to protect the reactive portion of NADH from solvent. In the presence of the isonicotinic acyl group, the side chain of Phe^{149} has rotated away from the nicotinamide ring, creating space for the isonicotinic acyl group. In addition, the side chain of Phe^{149} is now oriented adjacent to the pyridine ring of the isonicotinic acyl group, allowing it to participate in an aromatic ring-stacking interaction. Produced with the program Insight (*32*).

solution or within KatG) because an incubation mixture containing all the reaction components, except InhA, does not produce a detectable amount of isonicotinic acyl-NADH (*24*).

The crystal structure of isoniazid-inhibited InhA provides an explanation for the exquisite specificity of activated isoniazid for InhA. The location and orientation of the isonicotinic acyl group are complementary to those of the surrounding InhA side chains, which create a specific binding pocket for the isonicotinic acyl group (Fig. 4). In addition, the size and shape of the pocket could accommodate the isoniazid analog ethionamide. Although KatG is not the activator of ethionamide (*13*), ethionamide also requires activation and, by analogy to isoniazid, we propose that activated ethionamide inhibits InhA by becoming covalently attached to position four of the nicotinamide ring of NADH by a 2-ethyl isonicotinic thioacyl group.

Comparison of the crystal structures of InhA with bound NADH (*18*) and with bound isonicotinic acyl-NADH reveals that the only significant difference in the protein is location of the side chain of Phe^{149} (Fig. 5). When isonicotinic acyl-NADH is bound, the side chain of Phe^{149} has rotated ~90° and forms an aromatic ring-stacking interaction with the pyridine ring of the isonicotinic acyl group. Although a binding constant that describes the affinity of InhA for isonicotinic acyl-NADH has not been determined, this new structural arrangement would increase the affinity over NADH alone. Similarly, mutations with decreased affinity for NADH (such as S94A) are likely to possess decreased affinity for isonicotinic acyl-NADH.

The existence of the isonicotinic acyl-NADH inhibitor, the affinity of InhA for NADH, and the order in which NADH and acyl-ACP substrates bind InhA now become critical to explaining InhA-related isoniazid susceptibility and resistance in *M. tuberculosis*. Kinetic isotope analysis of InhA has demonstrated that the binding sequence of NADH and long-chain acyl-ACP substrates is not strictly ordered, but there is a preference for NADH binding first (*6*). This preference would leave most of the wild-type enzyme in the NADH-bound form, available for attack by activated isoniazid. If wild-type InhA cannot release significant amounts of isonicotinic acyl-NADH, this will effectively create permanent inhibition of the enzyme and prevent mycolic acid biosynthesis. In contrast, the decreased affinity of the S94A mutant for NADH would promote acyl-ACP substrates binding before NADH, thereby protecting most of the enzyme from activated isoniazid. When the isonicotinic acyl-NADH is formed on the mutant enzyme, the lowered affinity for NADH promotes release of isonicotinic acyl-NADH, allowing normal substrate catalysis to proceed and resulting in isoniazid-resistant tuberculosis.

The mechanisms of drug action and drug resistance presented here for isoniazid are quite different from those predicted for isoniazid by analogy to diazaborine attachment to the 2′-hydroxyl oxygen of the nicotinamide ribose of the NAD^+ of the *Escherichia coli* enoyl-ACP reductase (FabI) (*25*). The crystal structure of the complex between isonicotinic acyl-NADH and InhA provides a basis for the design of agents that inhibit InhA without the need for KatG drug activation. The pathway of mycolic acid biosynthesis is essential to mycobacteria and therefore InhA is a logical choice for the design of drugs that control growth of *M. tuberculosis*.

Table 1. Data collection and model refinement statistics: space group $P6_222$; lattice constants, $a = b = 100.53$ Å, $c = 138.96$ Å, $\alpha = \beta = 90.0°$, and $\gamma = 120.0°$; rms, root mean square. Completeness = (number of $F_{observed}$/number of $F_{expected}$) × 100; $R_{sym} = [\Sigma|(I - \langle I\rangle)|/\Sigma(I)] \times 100$; average $I/\sigma I = \Sigma(I/\sigma I)$/number of I; R value = $[\Sigma(|F_{observed} - F_{calculated}|)/\Sigma(F_{observed})] \times 100$; R_{free} = R value of 10% of the data omitted at random.

	Overall	Highest shell
Resolution Å	10.00 to 2.70	2.77 to 2.70
Unique reflections	10,621	394
Completeness (%)	91	50
R_{sym} based on I (%)	16.4	34.3
Average $I/\sigma I$	11.3	2.4
R value (%)	20.2	27.8
R_{free} (%)	29.7	43.3
	Number of nonhydrogen atoms	Temperature factor (Å^2)
Protein main chain	1072	21.3
Protein side chain	922	23.3
Isonicotinic acyl-NADH	52	22.5
Ordered water molecules	68	30.6
		rms deviation from ideal
Bond length (Å)		0.01
Bond angles (°)		1.9
Dihedral angles (°)		26.1
Improper angles (°)		2.2

REFERENCES AND NOTES

1. R. J. O'Brien, in *Lung Biology in Health and Disease*, L. B. Reichman and E. S. Hershfield, Eds. (Dekker, New York, 1993), vol. 66, pp. 207–240.
2. B. A. Bloom, *Tuberculosis: Pathogenesis, Protection, and Control* (American Society for Microbiology, Washington, DC, 1994).
3. J. D. H. Porter and K. P. W. J. McAdam, *Annu. Rev. Public Health* **15**, 303 (1994); F. A. Drobniewski *et al.*, *J. Med. Microbiol.* **43**, 85 (1985).
4. D. B. Young, *Curr. Biol.* **4**, 351 (1994); Y. Zhang and D. Young, *J. Antimicrob. Chemother.* **34**, 313 (1994); S. T. Cole and A. Telenti, *Eur. Respir. J.* **8** (suppl. 20), 701s (1995); D. B. Young and K. Duncan, *Annu. Rev. Microbiol.* **49**, 641 (1995); J. S. Blanchard, *Annu. Rev. Biochem.* **65**, 215 (1996); B. Heym *et al.*, *Curr. Top. Microbiol. Immun.* **215**, 49 (1996).
5. A. Banerjee *et al.*, *Science* **263**, 227 (1994).
6. A. Quemard *et al.*, *Biochemistry* **34**, 8235 (1995).
7. P. J. Brennan and H. Nikaido, *Annu. Rev. Biochem.* **64**, 29 (1995); R. E. Lee *et al.*, *Curr. Top. Microbiol. Immunol.* **215**, 1 (1996).
8. F. G. Winder and P. B. Collins, *J. Gen. Microbiol.* **63**, 41 (1970); K. Takayama *et al.*, *Antimicrob. Agents Chemother.* **2**, 29 (1972); L. Wang and K. Takayama, *ibid.*, p. 438; K. Takayama *et al.*, *J. Lipid Res.* **16**, 308 (1975); L. A. Davidson and K. Takayama, *Antimicrob. Agents Chemother.* **16**, 104 (1979); A. Quemard *et al.*, *ibid.* **35**, 1035 (1991); P. R. Wheeler and P. M. Anderson, *Biochem. J.* **318**, 451 (1996); K. Mdluli *et al.*, *J. Infect. Dis.* **174**, 1085 (1996).
9. J. C. Sacchettini and J. S. Blanchard, *Res. Microbiol.* **147**, 36 (1996).
10. A. Quemard *et al.*, *J. Am. Chem. Soc.* **118**, 1561 (1996).
11. R. F. Zabinski and J. S. Blanchard, *ibid.* **119**, 2331 (1997).
12. R. S. Magliozzo and J. A. Marcinkeviciene, *J. Am. Chem. Soc.* **118**, 11303 (1996); *J. Biol. Chem.* **272**, 8867 (1997).
13. K. Johnson *et al.*, *J. Am. Chem. Soc.* **117**, 5009 (1995); L. A. Basso *et al.*, *ibid.* **118**, 11301 (1996).
14. M. Y. Stoeckle *et al.*, *J. Infect. Dis.* **168**, 1063 (1993); B. Heym *et al.*, *Lancet* **344**, 293 (1994); B. Heym *et al.*, *Mol. Microbiol.* **15**, 235 (1995); F. R. Cockerill *et al.*, *J. Infect. Dis.* **171**, 240 (1995); V. Kapur *et al.*, *Arch. Pathol. Lab. Med.* **119**, 131 (1995); D. A. Rouse *et al.*, *Antimicrob. Agents Chemother.* **39**, 2472 (1995); J. M. Musser *et al.*, *J. Infect. Dis.* **173**, 196 (1996); A. Telenti *et al.*, *J. Clin. Microbiol.* **35**, 719 (1997).
15. Y. Zhang *et al.*, *Nature* **358**, 591 (1992); Y. Zhang *et al.*, *Mol. Microbiol.* **8**, 521 (1993).
16. K. Johnson and P. G. Schultz, *J. Am. Chem. Soc.* **116**, 7425 (1994).
17. J. M. Musser, personal communication.
18. A. Dessen *et al.*, *Science* **267**, 1638 (1995).
19. Isoniazid-inhibited InhA was produced by incubating at room temperature 350 μM InhA, 17.5 mM NADH,

35 mM isoniazid, and 3.5 mM $MnCl_2$, buffered at pH 7.5 with 50 mM Hepes. Before InhA was added to the reaction mixture, it was stored in 1 mM EDTA, 1 mM dithiothreitol, and 0.5 mM phenylmethylsulfonyl fluoride, buffered at pH 7.5 with 50 mM Hepes. InhA activity was measured by removing aliquots from the incubation mixture and spectrophotometrically monitoring the turnover of fresh NADH to NAD^+ at 340 nm in the presence of a fatty acyl-CoA substrate (6). InhA activity decreased by 90% within 2 days and coincided with the reaction mixture turning bright yellow. Crystals of isoniazid-inhibited InhA were produced by combining the incubation mixture in a 1:1 ratio with 12% methyl pentane diol, 4% dimethyl sulfoxide, 100 mM Hepes at pH 7.5, and 50 mM sodium citrate at pH 6.5, and placing it in a hanging drop enclosure. Within a week, crystals reached a size of 0.4 × 0.3 × 0.3 mm and were of the same morphology as those used previously to determine the native crystal structure (*18*).

20. A single crystal was used to collect a data set at room temperature with a MacScience DIP2030 image plate system with double-focusing mirrors coupled to a Rigaku x-ray generator, using a copper rotating anode with a 0.005-mm nickel filter and a 0.5-mm x-ray beam collimator. The Denzo and Scalepack package (*26*) was used to autoindex, integrate, and scale frames of data. Data collection statistics are listed in Table 1.
21. An initial difference Fourier ($F_o - F_c$) electron density map, in which the calculated phases were derived from the native InhA model with bound NADH (PDB 1eny), contained a single intense peak (7σ) with a size and shape distinctive of the isonicotinic acyl group derived from isoniazid. No other peaks existed in the map with the same intensity and characteristics. Refinement of the isoniazid-inhibited InhA model was performed with the X-PLOR software package (*27*) and a 2σ cutoff was applied to the structure factors, resulting in less than 2% of the data being omitted. Several rounds of manual model building and automated refinement with addition of the isonicotinic-acyl group and 68 ordered water molecules brought the R_{factor} to 20.2% and the R_{free} to 29.7% for data from 10.0 to 2.7 Å. Throughout this process, the validity of the model was confirmed by inspecting simulated annealing omit maps, in which either 10 contiguous residues or a 6 Å sphere was omitted. Model refinement statistics are listed in Table 1.
22. Before mass spectrometry, the isoniazid-inhibited InhA was separated from the other components of the reaction mixture (excess NADH, isoniazid, Mn^{2+} ions) by using a Pharmacia Superdex-75 HR-10/30 gel-filtration column equilibrated in 100 mM triethylammonium acetate, pH 7.0, at a flow rate of 0.5 ml/min. The fractions containing the isoniazid-inhibited InhA were pooled and concentrated to about 2 mg/ml. An enzymatic activity assay confirmed that the purified protein was inactive, which implies that the isonicotinic acyl-NADH was still bound to InhA. Portions of this enzyme preparation (10 to 20 μl) were brought to 100 μl with a solution of 50% methanol and 1% acetic acid in water. These dilutions were infused into a Finnigan LCQ electrospray mass spectrometer at 5 μl/min. Spectra were analyzed in positive mode and averaged for 1 min. The mass value of 770 daltons obtained for the isonicotinic acyl-NADH, present within the isoniazid-inhibited InhA sample, corresponds to the addition of a mass fragment consisting of NADH with one hydrogen removed (mass = 664 daltons) plus a mass fragment consisting of an isonicotinic acyl group derived from isoniazid (mass = 106 daltons).
23. H. A. Shoeb *et al.*, *Antimicrob. Agents Chemother.* **27**, 399 (1985).
24. Reaction mixtures containing Mn^{2+} ions, [*ring*-^{14}C]-isoniazid, and NADH (or NAD^+) with and without InhA were applied to a Pharmacia Superdex-Peptide gel-filtration column and equilibrated in 50 mM Hepes, pH 7.5, at a flow rate of 0.5 ml/min. Each component of the starting mixture was separated and identified, and the radioactivity of each column fraction was measured in a scintillation counter. Incubations that lack InhA do not shift any portion of the radiolabel from the isoniazid peak to an area of the chromatogram of larger molecular mass near the NADH peak.
25. C. Baldock *et al.*, *Science* **274**, 2107 (1996).
26. Z. Otwinowski, in *Data Collection and Processing*, L. Sawyer, N. Isaacs, S. Bailey, Eds. [Science and Engineering Research Council (SERC), Daresbury Laboratory, Warrington, UK, 1993], pp. 56–62.
27. A. T. Brunger, *X-PLOR version 3.1, A System for X-Ray Crystallography and NMR* (Yale Univ. Press, New Haven, CT, 1992).
28. F. Paoletti *et al.*, *Chem.-Biol. Interactions* **76**, 3 (1990).
29. E. Lewin and J. G. Hirsh, *Am. Rev. Tuberc. Pulm. Dis.* **71**, 732 (1955); F. G. Winder and J. M. Denneny, *Biochem. J.* **73**, 500 (1959); K. Ito *et al.*, *Biochemistry* **31**, 11606 (1992).
30. H. A. Shoeb *et al.*, *Antimicrob. Agents Chemother.* **27**, 404 (1985); H. A. Shoeb *et al.*, *ibid.*, p. 408; A. Hillar and P. C. Loewen, *Arch. Biochem. Biophys.* **323**, 438 (1995).
31. B. K. Sinha, *J. Biol. Chem.* **258**, 796 (1983).
32. Figure 1 was made with the program O, version 5.9 (T. A. Jones and M. Kjeldgaard, Uppsala University, Uppsala, Sweden). Figures 3 and 4 were made with Chemistry 4-D Draw (ChemInnovation Software, San Diego, CA), and Fig. 5 was made with INSIGHT II (Biosym Technologies, San Diego, CA).
33. Financial support was provided by the Welch Foundation and NIH grants GM-45859 and AI-36849. We thank C. Vilcheze and R. Bittman for supplying 2-*trans*-octenoyl-coenzymeA for InhA activity assays, M. W. Crankshaw for mass spectrometry analysis, members of the Center for Structural Biology at Texas A&M University (http://reddrum.tamu.edu/vivek/Public) for helpful discussions, and M. Edwards for manuscript preparation assistance. The coordinates have been deposited in the Protein Data Bank with entry number 1zid.

16 May 1997; accepted 4 November 1997

Ultraviolet-Induced Cell Death Blocked by a Selenoprotein from a Human Dermatotropic Poxvirus

Joanna L. Shisler, Tatiana G. Senkevich, Marla J. Berry, Bernard Moss*

Selenium, an essential trace element, is a component of prokaryotic and eukaryotic antioxidant proteins. A candidate selenoprotein homologous to glutathione peroxidase was deduced from the sequence of molluscum contagiosum, a poxvirus that causes persistent skin neoplasms in children and acquired immunodeficiency syndrome (AIDS) patients. Selenium was incorporated into this protein during biosynthesis, and a characteristic stem-loop structure near the end of the messenger RNA was required for alternative selenocysteine decoding of a potential UGA stop codon within the open reading frame. The selenoprotein protected human keratinocytes against cytotoxic effects of ultraviolet irradiation and hydrogen peroxide, providing a mechanism for a virus to defend itself against environmental stress.

The trace element selenium is essential for survival, as demonstrated by the early embryonic lethality of targeted disruption of the selenocysteine (Sec) tRNA gene (*1*). Several lines of evidence, mostly based on a decrease or increase in dietary selenium, suggest that selenoproteins have roles in antioxidant defenses, thyroid function, reproductive capacity, and protection against tumors and virus infections (*2, 3*). Although selenoproteins are present in Bacteria, Archaea, and Eukarya, heretofore no viral selenoprotein has been demonstrated. A recent analysis of the DNA sequence of molluscum contagiosum virus (MCV) revealed an open reading frame (ORF), MC066L, with homology to human glutathione peroxidase (*4*), a well-characterized selenoenzyme that reduces cytotoxic peroxides (*2, 5*). The MCV contains more than 150 genes (*6*) and, like other poxviruses, replicates in the cytoplasm of infected cells (*7*). It resides exclusively in the human epidermis, where it causes persistent, benign neoplasms in children and essentially untreatable opportunistic infections in AIDS patients (*8*). Apoptosis plays an important role in the biology of the epidermis and may provide a mechanism for regression of some epidermal neoplasms (*9*). The putative MCV glutathione peroxidase may protect infected cells against ultraviolet (UV) irradiation, which is known to induce apoptosis through the action of hydrogen peroxide and superoxide anions (*10*).

The MC066L ORF was predicted to encode a selenoprotein because of the presence of a potential UGA stop codon, which could be decoded as Sec, within the region of homology with glutathione peroxidase (*4*). Recognition of the Sec codon is relatively inefficient and depends on a secondary structural selenocysteine insertion sequence (SECIS) element, which occurs immediately after UGA

J. L. Shisler, T. G. Senkevich, B. Moss, Laboratory of Viral Diseases, National Institute of Allergy and Infectious Diseases, National Institutes of Health, 4 Center Drive, MSC 0445, Bethesda, MD 20892–0445, USA.
M. J. Berry, Thyroid Division, Harvard Institutes of Medicine, 77 Avenue Louis Pasteur, Boston, MA 02115, USA.
*To whom correspondence should be addressed.